GaN HEMT DC I-V Device Model for Accurate RF Rectifier Simulation

doi: 10.1109/LMWC.2017.2746678

GaN HEMT DC I-V Device Model for Accurate RF Rectifier Simulation

Tsukasa Yasui, Ryo Ishikawa, *Member, IEEE,* and Kazuhiko Honjo, *Fellow, IEEE*

***Abstract*—Recently, various high-efficiency RF rectifiers have been proposed. In this article, to improve the simulation accuracy of RF active rectifier circuits, a new device model for GaN HEMTs is proposed that improves the reproducibility of I_D-V_{DS} characteristics in the third-quadrant region (both drain voltage and drain current are negative). Based on measured characteristic data of an actual GaN HEMT, the device parameters for this model have been decided, and the advantage of the new device model has been confirmed.**

***Index Terms*—GaN HEMT, RF rectifier, device model, third-quadrant region.**

I. Introduction

VARIOUS wireless power transmission systems have been proposed for several applications, such as remote sensing, wireless battery charging, and so on [1]–[3]. In recent years, various high-efficiency rectifiers using an active device such as a GaN HEMT have been proposed [4], [5]. Usually, such high-efficiency active rectifiers are designed using an RF circuit simulator. On the other hand, an active device in high-efficiency rectifiers works in the "third-quadrant" region, in which a reverse drain (or collector) voltage is applied and a reverse drain current flows. Especially, DC-to-RF/RF-to-DC interconversion systems [6] use both the first-quadrant and third-quadrant regions of an active device. However, such an operating mode of active devices is not seen in most other kinds of RF circuits, so simulation device models are considered to have insufficient reproducibility accuracy in the third-quadrant region. Raffo et al. [13] show that microwave intrinsic transistor characteristics can be expressed by nonlinear capacitive elements and nonlinear DC characteristics. In this letter, we attempt improving the DC characteristics of the device model, especially, third-quadrant region. It will improve the overall RF accuracy of the device model.

The look-up table approach [11] is a simple way to express nonlinear characteristics of active devices including third-quadrant region. In this approach, however, it is difficult to provide differentiable functions including higher order derivatives based on measured data. This is important problem to simulate high-efficiency rectifiers using harmonic treatment technique.

In this paper, first, the reproducibility accuracy of the EEHEMT1 device model on the third-quadrant region is shown by measuring and modeling for an actual GaN HEMT, then an improvement method for reproducibility is shown.

II. I_D-V_{DS} Characteristics Expression on EEHEMT1 Device Model

Keysight Technologies' EEHEMT1 device model is one of the common simulation models for HEMT devices in the RF/Microwave field. Fig. 1 shows the internal equivalent circuit of the EEHEMT1 device model [7]. In Fig. 1, drain

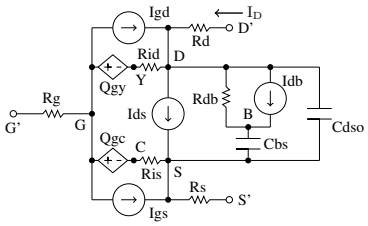

Fig. 1. EEHEMT1 internal equivalent circuit.

current I_D is expressed some current sources. Ids generates a dominant DC drain current that depends on gate-source voltage V_{GS} and drain-source voltage V_{DS}, Igd and Igs express the gate forward and breakdown currents, respectively. Though Idb, Rdb, and Cbs express the dispersion effects at low frequencies, it is not enough to express the complicated dispersion effects in GaN HEMTs [12]. Even so, at least more accurate DC model is needed to express these effects. In the EEHEMT1 device model, Ids', the no thermal effect version of Ids, can be expressed by three terms, namely, U, V, and W, as follows:

$$\begin{cases} Ids' = U \cdot V \cdot W \\ U = I_{dso}^{comp}(V_{GS}, V_{DS}) \\ V = 1 + KAPA \cdot V_{DS} \\ W = tanh(\frac{3V_{DS}}{VSAT}) \end{cases} \tag{1}$$

where U or I_{dso}^{comp} is a complicated function with respect to V_{GS} and V_{DS}, V is obviously a linear function with respect to V_{DS}, and W represents the saturation effect of drain current by $tanh$ function [8], [9]. Finally, Ids is derived from Ids' with taking the thermal effect, as shown by

$$Ids = \frac{Ids'}{1 + \frac{P_{diss}}{PEFF}} \tag{2}$$

where P_{diss} is the power dissipation of the device due to Ids' and V_{DS}, and $PEFF$ is a device model parameter that determines the thermal effect of the device. The Ids must be a differentiable function, and its derivatives should ideally also be differentiable up to an infinite order. The Ids of the EEHEMT1 device model is described as a continuous function of at least 2nd order derivatives. Equation (1) is only used for

the first-quadrant region. For the third-quadrant region, the following equation is used instead of (2).

$$Ids_{(V_{DS}<0)} = -Ids(V_{GS} - V_{DS}, -V_{DS}) \tag{3}$$

Equation (3) expresses the I_D-V_{DS} characteristics in the third-quadrant region using the first-quadrant expression and the same device model parameters based on the terminal transformation technique with the device symmetry assumption, as shown by Fig. 2. This simple symmetry assumption provides

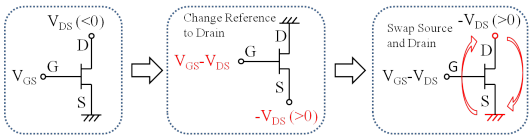

Fig. 2. Transform the third-quadrant region to first-quadrand region.

a reasonable way to obtain the approximate characteristics in the third-quadrant region for most RF applications. However, in almost all actual FET devices such as GaN HEMTs, its structure is not symmetrical for improvement of the drain breakdown voltage [10]. This means that (3) does not give accurate characteristics in the third-quadrant region. Thus, for active RF rectifier simulation, more accurate device model is needed to provide more accurate characteristics in that region.

III. Comparison of Measured Characteristics and EEHEMT1 Device Model

In order to understand the reproducibility of the characteristics in the third-quadrant region, we measured the I_D-V_{DS} characteristics of an actual GaN HEMT device (WIN semiconductors' 4×100μm gate width) based on stationary mode measurement. Then, we attempted to decide the parameters for the EEHEMT1 device model. As a result, it was impossible to fit the measured I_D-V_{DS} curves to the EEHEMT1 model in both the first-quadrant region and the third-quadrant region. The result of model fitting is shown in Fig. 3. In this result, the

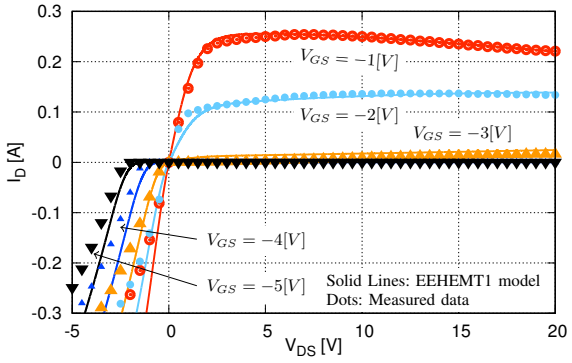

VTO=-3.75[V], GAMMA=590.9 × 10^{-6}[V^{-1}], VGO=-1.882[V], VDELT=50.0 × 10^{-3}[V], VCH=3.345[V], GMMAX=138.4 × 10^{-3}[S], VDSO=8.0[V], VSAT=4.071[V], KAPA=36.28 × 10^{-3}[V^{-1}], PEFF=8.671[W] Unless otherwise specified, default values are used.

Fig. 3. Measured I_D-V_{DS}, simulation result using EEHEMT1 model, and model parameters.

fitted EEHEMT1 model shows good approximation in the first-quadrant region, however, a difference was observed between the model and measured data in the third-quadrant region. The assumption of device symmetry is considered to be one of the reasons for this difference. To improve this mismatch, we introduced a new function named V' instead of V in (1).

$$V' = 1 + KAPA \cdot V_{DS} + \frac{1}{A \cdot (PHI - V_{GS})^{B+D \cdot V_{GS}}} \cdot \tanh(\frac{V_{DS}}{C} - 1) \tag{4}$$

This equation corrects the Ids in the third-quadrant region for better approximation, but there is almost no effect on other regions. In (4), each A, B, and D is the parameter that determines the influence of V_{GS} on Ids. C is the roll-off factor of V' around $V_{DS} = 0$. A small offset PHI prevents the divergence of V' on $V_{GS} \geq 0$. In addition, in (4) the device symmetry assumption expressed as (3) is not applied. In other words, each V_{GS} and V_{DS} in (4) means the actual gate and drain voltage, respectively, even in the third-quadrant region. A comparison example between V and V' is shown in Fig. 4. Equation (4) is a differentiable function with respect to V_{GS}

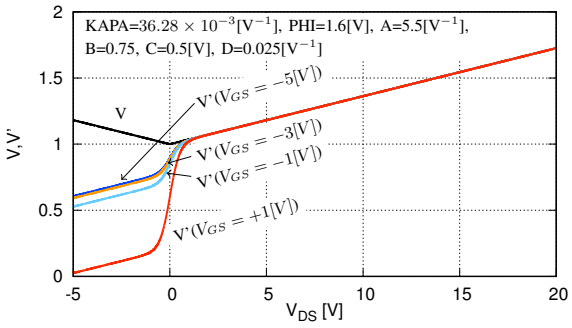

Fig. 4. Plot example for V and V' respectively.

and V_{DS} with $V_{GS} < PHI$, and at least 2nd order derivatives are also differentiable with $V_{GS} < PHI$, as shown in the following equation:

$$\frac{\partial V'}{\partial V_{DS}} = KAPA + \frac{1}{AC(PHI - V_{GS})^{B+D \cdot V_{GS}}} \cdot \left\{1 - \tanh^2(\frac{V_{DS}}{C} - 1)\right\} \tag{5}$$

$$\frac{\partial^2 V'}{\partial V_{DS}^2} = -\frac{2}{AC^2(PHI - V_{GS})^{B+D \cdot V_{GS}}} \cdot \tanh(\frac{V_{DS}}{C} - 1)\left\{1 - \tanh^2(\frac{V_{DS}}{C} - 1)\right\} \tag{6}$$

$$\frac{\partial V'}{\partial V_{GS}} = -\frac{1}{A(PHI - V_{GS})^{B+D \cdot V_{GS}}} \cdot \left\{D \cdot \ln(PHI - V_{GS}) - \frac{B+D \cdot V_{GS}}{PHI - V_{GS}}\right\} \cdot \tanh(\frac{V_{DS}}{C} - 1) \tag{7}$$

$$\frac{\partial^2 V'}{\partial V_{GS}^2} = \frac{1}{A(PHI - V_{GS})^{B+D \cdot V_{GS}}} \cdot \left[\left\{D \cdot \ln(PHI - V_{GS}) - \frac{B+D \cdot V_{GS}}{PHI - V_{GS}}\right\}^2 + \frac{B+D \cdot V_{GS}}{(PHI - V_{GS})^2} + \frac{2D}{PHI - V_{GS}}\right] \cdot \tanh(\frac{V_{DS}}{C} - 1) \tag{8}$$

IV. Fitting Result Using the Improved Model

Using V' instead of V in (1), we produced an improved version of the EEHEMT1 device model. The fitting result for

the actual device which is described in section III, is shown in Fig. 5.

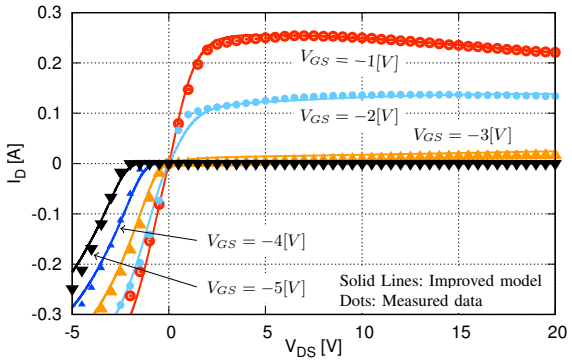

A=5.5[V^{-1}], B=0.75, C=0.5[V], D=0.025[V^{-1}], PHI=1.6[V]
Unless otherwise specified, values shown in Fig. 3 are used.

Fig. 5. Measured I_D-V_{DS}, simulation result using the improved model, and model parameters.

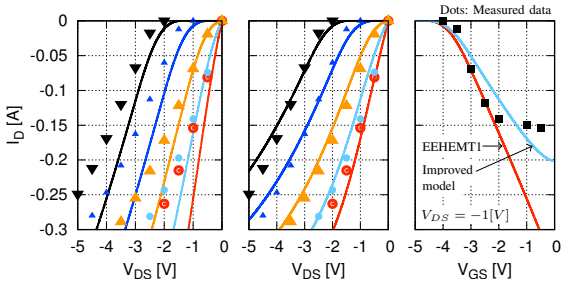

(a) Details of Fig. 3 (b) Details of Fig. 5 (c) V_{GS}-I_D

Fig. 6. Details of the third-quadrant region characteristics.

The improved device model gives good approximation in the third-quadrant region without a large effect in the first-quadrant region, as shown in Fig. 6 and Fig. 7. Fig. 8 shows an example for 1GHz active RF rectifier design. Fig. 9 shows the time-domain simulation result. In this simulation, the power conversion efficiency was 58.9% for EEHEMT1 model and 49.7% for improved model, respectively.

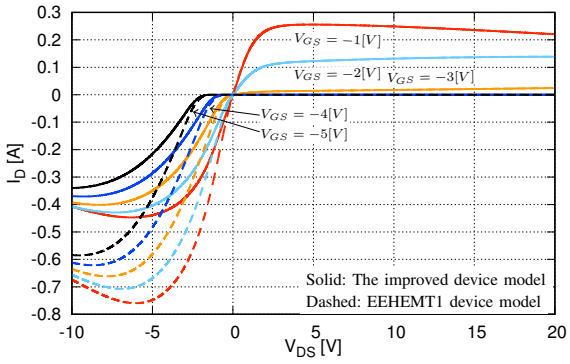

Fig. 7. Difference between EEHEMT1 and the improved model.

V. Conclusion

We described the reproducibility of the EEHEMT1 device model in the third-quadrant region, and proposed an improved device model. The improved device model gives better I_D-V_{DS} curves in the third-quadrant region without much effect in the first-quadrant region. This would be helpful in the design of high-efficiency active rectifiers.

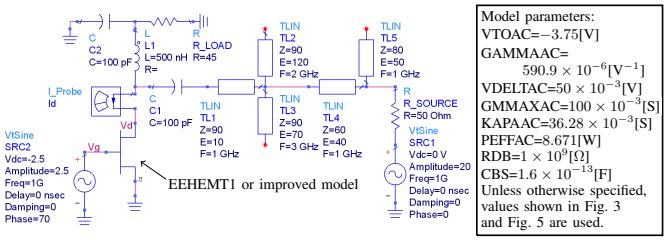

Fig. 8. 1GHz active RF rectifier simulation circuit.

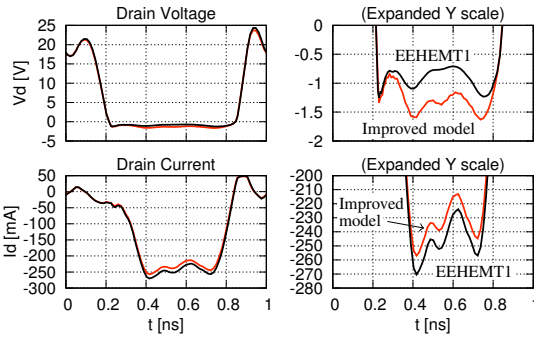

Fig. 9. Time-domain waveforms of the 1GHz active RF rectifier simulation.

References

[1] N. Tesla, "Apparatus for transmitting electrical energy," U.S. Patent 1 119 732, Dec. 1, 1914.
[2] A. Kurs *et al.*, "Wireless power transfer via strongly coupled magnetic resonances," *Science Mag.*, vol. 317, no. 5834, pp. 83–86, Jul. 2007.
[3] W. C. Brown *et al.*, "Microwave to DC converter," U.S. Patent 3 434 678, Mar. 25, 1969.
[4] C. Gómez *et al.*, "A high efficiency rectenna element using E-pHEMT technology," in *Proc. 12th GaAs Symp.*, Oct. 2004, pp. 315–318.
[5] I. Ramos *et al.*, "GaN Microwave DC-DC Converters," *IEEE Trans. Microw. Theory Techn.*, vol. 63, no. 12, pp. 4473–4482, Dec. 2015.
[6] R. Ishikawa, and K. Honjo, "High-efficiency DC-to-RF/RF-to-DC inter-conversion switching module at C-band," in *Proc. 2015 European Microw. Conf.*, Sep. 2015, pp. 295–298.
[7] *Agilent 85190A IC-CAP 2006 Reference*, Agilent Technologies Inc., Palo Alto, CA, 2006, pp.787–812.
[8] W. R. Curtice, "A MESFET model for use in the design of GaAs integrated circuits," *IEEE Trans. Microw. Theory Techn.*, vol. 28, no. 5, pp. 448–456, May 1980.
[9] I. Angelov, H. Zirath, and N. Rorsman, "A New Empirical Nonlinear Model for HEMT and MESFET Devices," *IEEE Trans. Microw. Theory Techn.*, vol. 40, no. 12, pp. 2258–2266, Dec. 1992.
[10] T. Furutsuka, T. Tsuji, and F. Hasegawa, "Improvement of the Drain Breakdown Voltage of GaAs Power MESFET's by a Simple Recess Structure," *IEEE Trans. Electron. Devices*, vol. ED-25, no. 6, pp.563–567, Jun. 1978.
[11] G. Crupi *et al.*, "Nonlinear modeling of GaAs pHEMTs for millimeter-wave mixer design," *Solid State Electron.*, vol. 104, no. 2, pp. 25–32, Feb. 2015.
[12] O. Mitrofanov, and M. Manfra, "Mechanisms of gate lag in GaN/AlGaN/GaN high electron mobility transistors," *Superlattices Microstruct.*, vol. 34, nos. 1–2, pp. 33–53, 2003.
[13] A. Raffo, F. Scappaviva, and G. Vannini, "A new approach to microwave power amplifier design based on the experimental characterization of the intrinsic electron-device load line," *IEEE Trans. Microw. Theory Tech.*, vol. 57, no. 7, pp. 1743-1752, Jul. 2009.